fixation cross was presented during the interval and the delay period. In addition, a visual cue (changing the color of the fixation cross) was presented for 500 ms prior to trial onset. Auditory cues (1000 and 800 Hz pure tones of 100-ms duration) were presented at the onsets of the visual cue and S2, respectively.

In the verbal WM task, four Japanese characters in *Hiragana* were presented as S1, and a Japanese character in *Katakana* was presented as S2. The participants were instructed to judge whether the character presented as S2 corresponded to any of the characters in S1 and then to press the appropriate button. Because the characters in S1 and S2 were presented in different Japanese morphograms (i.e., *Hiragana*/*Katakana*), participants were prompted to make their judgments based on the phonetic information of the characters, not by their form. In the spatial WM task, S1 was the location of four red squares out of eight locations, and S2 was the location of a red square. The participants' task was to assess if the location of the red square presented as S2 was identical to any of the locations of the four red squares presented in S1.

Each WM task had two additional conditions: Eriksen flanker tasks (Eriksen and Eriksen, 1974) were embedded in the delay period as distracter stimuli. These conditions were irrelevant to the purpose of the present study, so they were not included in the analysis.

2.4. Procedure

Participants were seated in a comfortable chair in a dim, quiet room. Their moods were assessed with a short form of the POMS questionnaire (Japanese version) (Yokoyama et al., 1990) at the beginning of the experiment. Next, they received computer-automated instructions that were followed by a brief practice session to familiarize them with the tasks. Thereafter, OT measurements were conducted while the participants performed the WM tasks. The tasks were organized into two sessions, one for the verbal WM task and the other for the spatial WM task, with a counterbalanced order across participants. Each session included five trials of either one of the tasks, and the sessions were separated by a short break (approximately 1 min). After the measurements, the participants completed a brief questionnaire that assessed their feelings about the experiments, which included subjective ratings of task difficulty on a 5-point scale, ranging from 1 ("not at all") to 5 ("extremely"). The duration of the OT measurements was approximately 15 min, and the whole experiment took about 45 min.

2.5. OT measurement

We used an OT system (ETG-4000, Hitachi Medical Corporation, Japan) equipped with 17 near-infrared light sources and 16 detectors. The light sources consisted of near-infrared continuous laser diodes with two wavelengths of 695 and 830 nm. The transmitted light was detected every 100 ms with avalanche photodiodes located 30 mm from the sources. These optodes (i.e., sources and detectors) were arrayed in a 3×11 lattice pattern and embedded in a soft silicon holder that was placed on the participant's forehead (Fig. 1B). This configuration formed 52 measurement points (defined as channels (Chs)), corresponding to each source-detector pair (Fig. 1C). The average power of each light source was 2 mW (for both wavelengths), and the sources were modulated at different frequencies (1–10 kHz) for wavelengths and sources so that signals from different measurement points could be discriminated.

To estimate the locations of the OT channels in the Montreal Neurological Institute (MNI) space and to generate 3-D topographical maps (Figs. 2 and 3), we used the probabilistic registration method (Okamoto and Dan, 2005; Singh et al., 2005). Prior to the experiment, we corrected the sample data for the three-dimensional coordinates of the 33 optode locations and scalp landmarks (in accordance with the international 10–20 system: Fp1, Fp2, Fz, T3, T4, C3, C4) for eight volunteers. The data were recorded with a 3D-magnetic space digitizer (3D probe positioning unit for OT system, EZT-DM101, Hitachi Medical Corporation, Japan).

2.6. Data analysis

Analyses were performed by means of plug-in-based analysis software, Platform for Optical Topography Analysis Tools (developed by Hitachi, ARL; run on MATLAB, The MathWorks, Inc., U.S.A.). First, we calculated the relative values of hemoglobin concentration changes (Hb-signals for oxy-Hb and deoxy-Hb) for each channel on the basis of the modified Beer-Lambert law, using light signals transmitted at the two wavelengths. The time-continuous data of Hb-signals for each channel were separated into task blocks, which were defined as a 25.5-s period starting from 1.0 s before S1 onset and ending 16.0 s after S2 onset, each containing a WM task trial. Next, blocks contaminated by motion artifacts were discarded. Although previous OT studies have used various methods to detect motion artifacts, no established method has been developed. Some studies used subjective methods based on visual inspection (Minagawa-Kawai et al., 2011), whereas others used objective methods (Orihuela-Espina et al., 2010; Takizawa et al., 2008). In this study, we used a criterion similar to (Pena et al., 2003): an oxy-Hb signal change larger than 0.4 mM mm over two successive samples (during 200 ms) was defined as a motion artifact. We found that this criterion effectively detected sharp noises (putatively unphysiological signal changes) identified by a visual inspection in our data, while maintaining the rejection rate at a low level (4.9%). The remaining data were baseline-corrected by linear regression based on the least squares method by using the data for the first 1.0 s the last 4.0 s of each block.

To evaluate the PFC activity during the tasks, we determined the *'activation period'* as being 3.5 s starting 5.0 s after S1 onset and ending on S2 onset (Fig. 2C). The onset of the activation period (5.0 s after S1 onset) was determined by taking into consideration the delay in hemodynamic changes from the neuronal activity. The offset of the activation period (immediately before S1 onset) was selected to avoid any confounding effects related to S2 presentation and the participant's response to the task. Because the activation period was entirely included in the 7.0-s WM-delay period, we expected that Hb-signals during this period would reflect cortical activity related to WM functions (i.e., encoding and maintenance) without it being affected by activity related to visual stimulation due to S2 or by body movement due to pressing buttons. Note that this time window was determined *a priori* and that the results reported here were not changed when we selected a longer time period (e.g., 5.0-s period starting 5.0 s after S1 onset; See Supplementary Fig. S1). The mean signal changes during the activation period, termed *'activation values,'* were calculated for both oxy-Hb and deoxy-Hb signals for each block. To assess the statistical significance of Hb-signal changes for the tasks, we first averaged the activation values within participants then performed a *t*-test (one sample, one-tailed) of the individual activation values against 0 across participants. For the between-task comparison of the activation values, we used a paired *t*-test (two-tailed) across participants.

To analyze the relationships of mood with task performance and PFC activity, we calculated the correlations between the POMS scores and behavioral measures or oxy-Hb signal changes for both WM tasks. We used Spearman's rank correlation because the relationships of subjective ratings with behavioral and neural measures are not necessarily regarded as linear (Schroeter et al., 2004).

All of these statistical analyses were performed for each channel. Therefore, when creating the statistical parametric map consisting of 52 channels, we used the false discovery rate (FDR) method to correct for multiple comparisons (Singh and Dan, 2006) with a threshold of FDR (q) < 0.05. Because FDR correction set a statistical threshold for each analysis, uncorrected *P*-values at thresholds were different across maps. Thus, the ranges of the statistical values (Student's t and Spearman's r, together with the thresholds of the uncorrected *P*-values) for the significant channels are presented for each statistical parametric map. Note that P denotes the uncorrected *P*-values for each channel and that q denotes the FDR for each map throughout this paper.

3. Results

3.1. POMS scores and subjective ratings

The mean and standard deviation (SD) of the POMS positive mood scores and negative mood scores were 8.76 ± 2.89 (ranging from 5 to 16) and 24.8 ± 14.5 (ranging from 3 to 56), respectively. These results are comparable to those obtained for a large sample of healthy Japanese adults (Yokoyama et al., 1990). The scores for male (9.18 ± 3.38 for positive mood scores, 22.8 ± 15.2 for negative mood scores) and female (8.17 ± 2.00 for positive mood scores, 27.6 ± 13.5 for negative mood scores) participants were not significantly different ($P = 0.556$ for positive mood scores, $P = 0.370$ for negative mood scores; Mann–Whitney *U*-test). The POMS positive mood scores and negative mood scores were not significantly correlated ($r = -0.28$, $P = 0.136$; Spearman's rank correlation).

The subjective ratings of task difficulty were 2.62 ± 0.90 for the verbal WM task and 2.93 ± 1.13 for the spatial WM task. The between-task difference was not significant ($P = 0.079$, Wilcoxon signed-rank test).

3.2. Behavioral performances

The mean reaction time (RT) for correct responses within individual participants was calculated for each WM task. The across-participants' mean and SD for RT were 1380 ± 239 ms for the verbal WM task and 1475 ± 270 ms for the spatial WM task. There were no significant differences between tasks ($t = -1.66$, $P = 0.108$, two-tailed paired *t*-test).

The number of correct responses ranged from three to five for both tasks, and the across-participants' mean and SD were 4.72 ± 0.59 for the verbal WM task and 4.31 ± 0.66 for the spatial WM task. Although this difference was relatively small (0.41), it was statistically significant ($P = 0.018$, Wilcoxon signed-rank test).

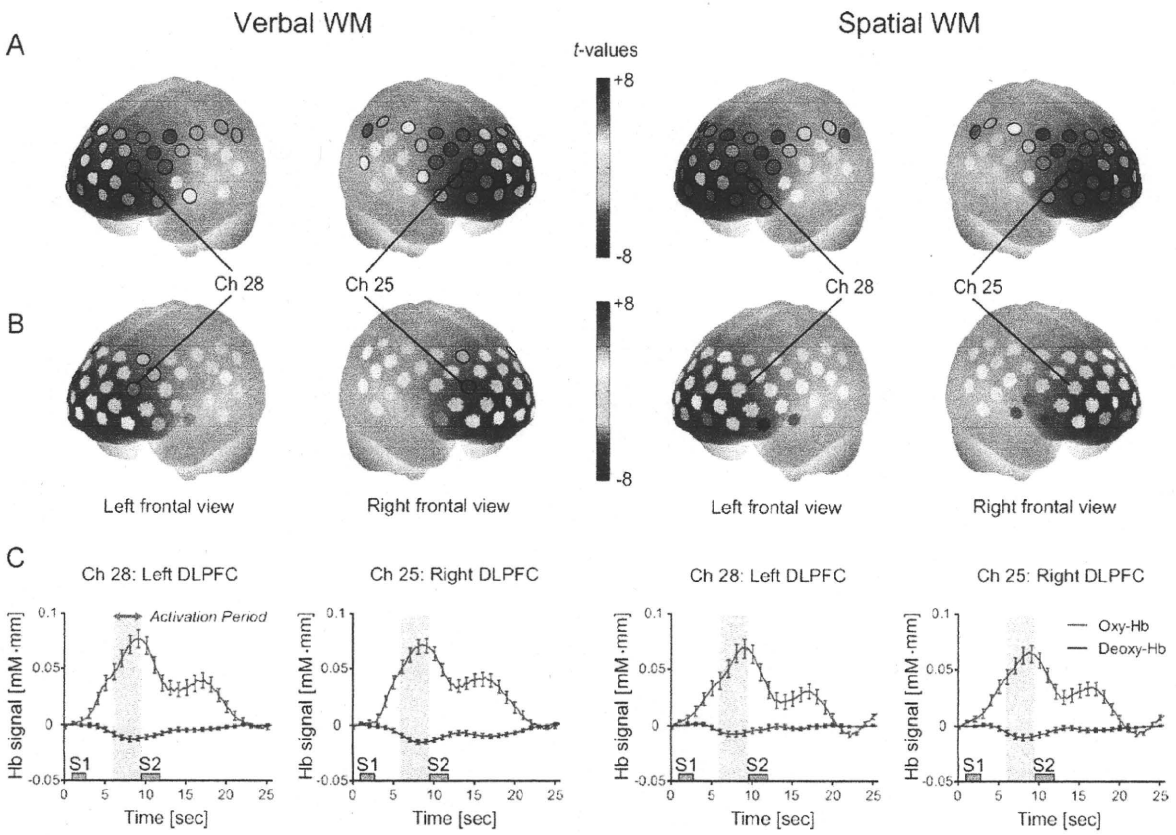

Fig. 2. Hemodynamic changes during verbal and spatial WM tasks. (A) Activation *t*-maps of oxy-Hb signal increase. (B) Activation *t*-maps of deoxy-Hb signal decrease. The Student's *t*-value is indicated by a color scale for each channel. Channels with significant *t*-values are marked with circles (FDR $q<0.05$). (C) Time courses for Hb-signal changes for representative channels (Chs 25 and 28 for right and left hemispheres, respectively). These time courses represent the grand average (with standard error bars) across all participants. The time spans (green bars perpendicular to *x*-axis) indicate activation period (3.5-s duration). Small rectangles (gray) indicate stimuli presentation time (S1, S2).

To determine whether participants' moods were associated with task performance, we calculated the correlation coefficients (Spearman's r) between the POMS scores and behavioral measures (accuracy and RT). A significant correlation was found only in the relationship between the POMS negative mood scores and RT for the verbal WM ($r=-0.37$, $P=0.046$), although this relationship was no longer significant after controlling for participants' age and gender ($r=-0.29$, $P=0.141$). No other significant correlation was evident between the POMS scores and behavioral measures ($r=-0.26$ to 0.20, $P>0.174$; see Supplementary Table).

3.3. PFC activity during WM tasks

First, we examined the across-participants' mean of the activation values for each WM task, without considering individual differences in the mood scores.

For both tasks, significant increases in the oxy-Hb signals (FDR $q<0.05$) were observed in a broad region of the PFC (Fig. 2A). For the verbal WM task, the oxy-Hb signals increased for 39 channels ($t=1.97$ to 6.55, $P<0.030$, $q<0.05$). Similarly, for the spatial WM task, the oxy-Hb signals increased for 36 channels ($t=2.10$ to 6.52, $P<0.024$, $q<0.05$).

Decreases in the deoxy-Hb signals were observed in a more localized region (Fig. 2B). For the verbal WM task, significant deoxy-Hb signal decreases were observed for five channels (Chs 25, 28, 18, 4, and 7; $t=-5.17$ to -3.03, $P<0.003$, $q<0.05$), two for the right hemisphere (Chs 4 and 25), and three for the left hemisphere (Chs 7, 18, and 28). The deoxy-Hb signal decreases for the spatial WM task were not significant at the FDR-corrected threshold. However, for reference, we found considerable decreases in the deoxy-Hb signals for the five channels (Chs 25, 18, 4, 8, and 28; $t=-2.82$ to -1.71, $P<0.05$ but $q>0.05$), two for the right hemisphere (Chs 4 and 25), and three for the left hemisphere (Chs 8, 18, and 28).

A comparison of the activation values between the verbal and spatial WM tasks revealed no significant differences in either the oxy-Hb signal increases or the deoxy-Hb signal decreases ($q>0.05$).

3.4. Temporal characteristics of oxy-Hb signal change

We analyzed the temporal characteristics of the oxy-Hb signal change based on the grand-averaged time course (Fig. 2C). For the channels where the oxy-Hb signal increases were significant during the activation period, the time courses for the oxy-Hb signal change had two peaks. The first (and the maximum) peak was observed during the delay period, and the second, more modest peak was observed after S2 was presented. We calculated the peak latency for the first peak, which was defined as the duration from S1 onset to the time the oxy-Hb signal reached a maximal value, and averaged this across channels with a significant oxy-Hb signal increase for both WM tasks. The mean of the peak latency was 7.81 ± 0.90 s for the verbal WM task and 7.61 ± 1.08 s for the spatial WM task. The difference between tasks was not significant ($t=1.82$, $df=35$, $P=0.077$, two-tailed paired *t*-test).

3.5. Correlation of POMS score with PFC activity

Next, to examine how the participants' moods were associated with the PFC activity during each WM task, we analyzed the correlation (Spearman's rank correlation) between the POMS scores

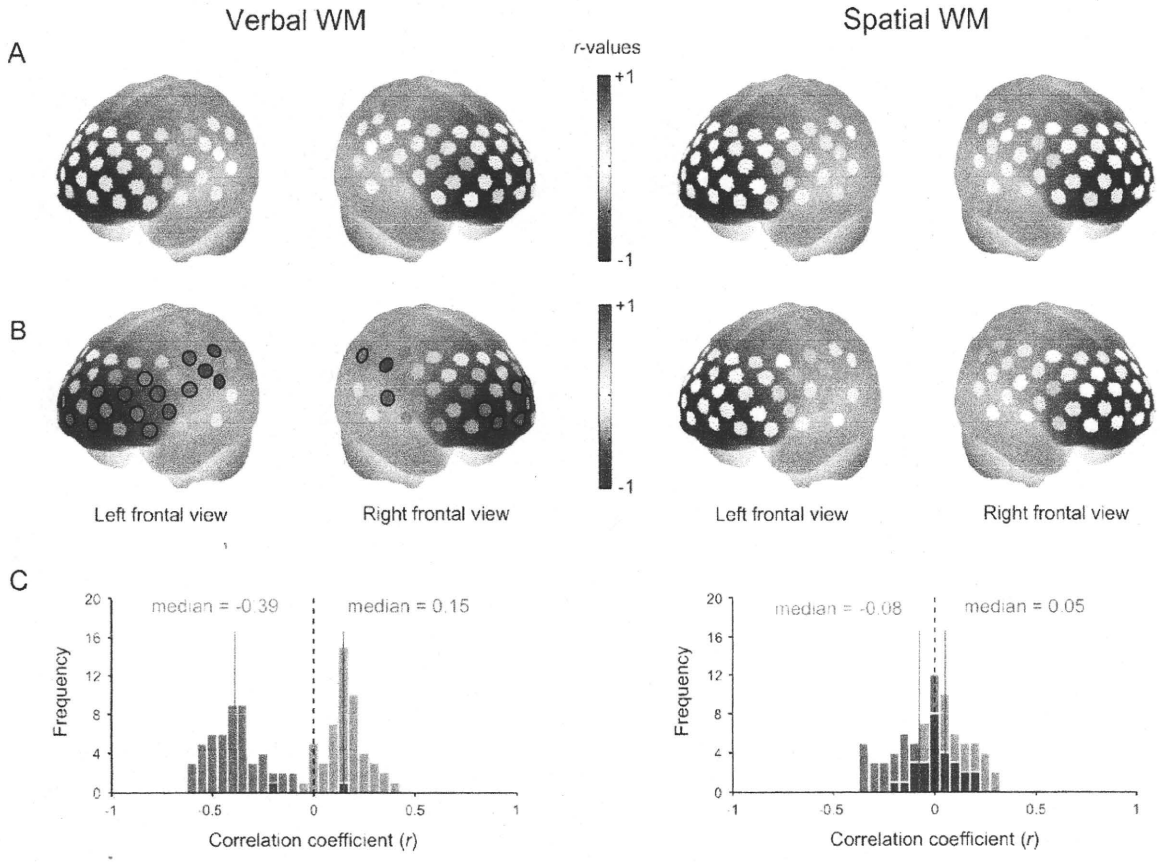

Fig. 3. Correlation between POMS scores and oxy-Hb signals. (A) Correlation *r*-maps showing relationship between POMS positive mood scores and oxy-Hb signal increase. (B) Correlation *r*-maps showing relationship between POMS negative mood scores and oxy-Hb signal increase. Left pairs: verbal WM task, right pairs: spatial WM task. The correlation coefficient (Spearman's *r*) is indicated by a color scale for each channel. Channels with statistical significance are marked with circles (FDR $q < 0.05$). (C) Histograms illustrate distributions of *r*-values for each *r*-map (Left: verbal WM, right: spatial WM). The vertical line indicates the median *r*-value among 52 channels consisting of a map. Red: correlation with POMS positive mood score, blue: correlation with POMS negative mood score.

and the activation values. We used only the oxy-Hb signal change because the deoxy-Hb signals did not show clear changes compared to the oxy-Hb signals (as described before).

For the verbal WM task, the oxy-Hb signal changes during the task tended to be positively correlated with the POMS positive mood scores (median *r*-value = 0.15, ranging from −0.21 to 0.40), whereas negatively correlated with the POMS negative mood scores (median *r*-value = −0.39, ranging from −0.62 to 0.16) (Fig. 3). We found statistically significant negative correlations between the POMS negative mood scores and the oxy-Hb signal changes for 19 channels ($r = -0.62$ to -0.44, $P = 0.0006$ to 0.017, $q < 0.05$) (Fig. 3B). Notably, the partial correlation analysis showed that a significant correlation remained in a specific channel (Ch 28; $r = -0.62$, $P = 0.0009$, $q < 0.05$) even when the participants' age, gender, and task performance (accuracy and RT) were controlled for. In addition, the correlation coefficients for the male ($n = 17$) and female ($n = 12$) participants were not significantly different in this channel ($r = -0.49$ for males, $r = -0.53$ for females; $P = 0.913$, Fisher's *Z*-test). The correlation plot for Ch 28 is shown in Fig. 4.

For the spatial WM task, the oxy-Hb signal changes during the task did not significantly correlate with either the POMS positive mood scores ($r = -0.20$ to 0.30, $P > 0.116$, $q > 0.05$) or negative mood scores ($r = -0.37$ to 0.21, $P > 0.056$, $q > 0.05$).

We also examined the correlations between task performance (accuracy and RT) and the oxy-Hb signal changes. Although there was a weak trend that higher accuracy was associated with a larger oxy-Hb increase in the frontopolar region for both verbal and spatial WM tasks ($r < 0.35$), no significant relationship was found (Supplementary Fig. S2).

4. Discussion

We measured the PFC activity during verbal and spatial WM tasks under low-constraint, near-natural conditions by using OT,

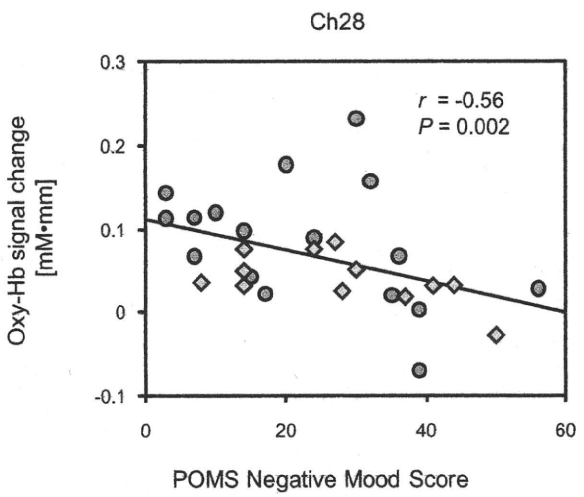

Fig. 4. Scatter plot showing relationship between POMS negative mood scores and PFC activity during verbal WM task in Ch 28. The negative correlation between the POMS scores and PFC activity was significant (FDR $q < 0.05$) in this channel, even after controlling for age, gender, and task performance. The blue circles indicate male participants, and the red diamonds indicate female participants. *r*: Spearman's rank correlation coefficient, *P*: uncorrected value. (For interpretation of the color information in this figure legend, the reader is referred to the web version of the article.)

to investigate the relationships between naturalistic mood and PFC activity. The results revealed statistically significant negative correlations between the POMS negative mood scores and PFC activity during the verbal WM task, whereas the opposite tendency was found for the POMS positive mood scores. However, the PFC activity during the task was not significantly correlated with either the POMS positive or negative mood scores for the spatial WM task. Our results indicate that even a normal range of mood variation in healthy individuals is associated with PFC activity during a WM task, suggesting a mood-cognition interaction under everyday circumstances manifested in PFC activity.

4.1. PFC activity induced by WM tasks

We observed a significant oxy-Hb signal increase in the PFC region in response to both verbal and spatial WM tasks. We did not observe a clear deoxy-Hb signal decrease comparable to the oxy-Hb signal increase, probably due to the lower signal to noise ratio. The decrease in the deoxy-Hb signal was significant only for the verbal WM task, but a similar spatial pattern was observed for the spatial WM task (Fig. 2B). An oxy-Hb signal increase accompanied by a deoxy-Hb signal decrease is considered to be a typical pattern of a hemodynamic response elicited by neuronal activity often observed in OT measurements (Herrmann et al., 2007; Sato et al., 2005, 1999). This pattern was found in the bilateral dorsolateral PFC, as identified by the probabilistic registration method (Okamoto and Dan, 2005; Singh et al., 2005). Therefore, we regarded these areas as activation foci responsible for WM functions. These results are consistent with those from previous research with other modalities (such as fMRI and PET), which have demonstrated DLPFC activation in response to performance of WM tasks (Gray et al., 2002; Smith and Jonides, 1999). Previous OT studies have also reported DLPFC activation during WM tasks (Hoshi et al., 2003; Tsujimoto et al., 2004). In particular, Tsujimoto et al. (2004), using the same delayed-response paradigm for the spatial WM task in our study, found that the oxy-Hb signal increase during the delay period was indeed WM-load dependent (two items vs. four items). This finding also supports that the PFC activity observed in our study can be regarded as WM related.

The PFC activity in response to the WM tasks was similar across the tasks not only in the spatial activation pattern (Fig. 2A and B) but also in the temporal characteristics (Fig. 2C), as shown by the analysis on peak latency. Although some previous studies found laterality in the PFC activity between verbal and spatial WM (Smith and Jonides, 1999; Smith et al., 1996) (i.e., relatively right dominant activation in spatial WM and left dominant activation in verbal WM), we did not observe significant differences in PFC activity between the tasks. One reason for this might be that we used a small number of trials for each condition, resulting in less sensitivity to differences in cortical responses between tasks. Whether OT can detect the lateralized PFC activity related to WM functions is a future issue to be investigated.

4.2. Relationship between negative mood and PFC activity associated with WM

We found a significant negative correlation between the POMS negative mood scores and the oxy-Hb signal increases—participants with higher levels of negative moods showed lower levels of PFC activity specifically during the verbal WM task. Of importance, this relationship was not explained by potential confounding factors such as age, gender, or task performance (i.e., accuracy and RT), as determined by partial correlation analysis. Particularly, the significant result in the partial correlation analysis was obtained in a channel located in the left DLPFC (Ch 28), where the WM-related activity (characterized by both the significant increase in the oxy-Hb signal and the significant decrease in the deoxy-Hb signal) was observed in the group-average analysis. Our results are consistent with the previous fMRI study by Qin et al. (2009), who reported that an induced negative mood attenuated DLPFC activity during a verbal WM task (numerical N-back task). The present study suggests that not only an induced negative mood but also a naturalistic negative mood is associated with PFC activity related to verbal WM function. Our results extend previous neuroimaging findings regarding the mood-cognition interaction to broader context under everyday circumstances: subjective moods during recent life situations are reflected in PFC activity responsive to cognitive tasks. The use of a low-constraint, less-stressful neuroimaging tool as well as a relatively short measurement time might have enabled us to probe the relationship between naturalistic mood and PFC activity sensitively.

We did not observe a significant association between performance (accuracy or RT) and mood scores or OT signals. Thus, it is unclear whether lower levels of PFC activity in participants reporting higher levels of negative moods indicate impoverished PFC reactivity to verbal WM or greater processing efficiency for verbal WM. However, we emphasize that our results are in line with previous OT studies showing that PFC activity during verbal fluency tasks is decreased in people who have higher levels of fatigue and sleepiness, apart from task performance (i.e., the effect of task performance on PFC activity was adjusted by multiple regression) (Suda et al., 2009, 2008). Collectively, these results including ours suggest that decreased PFC activity is a neural marker of higher negative mood (or lower motivation to engage in cognitive tasks), which could be more sensitive than behavioral measures. A more reliable relationship between behavioral measures and mood scores or PFC activity might be obtained if we increase the number of trials or use more difficult cognitive tasks.

One of the advantages of our study compared to the previous OT studies showing negative associations between PFC activity and levels of fatigue and sleepiness (Suda et al., 2009; Suda et al., 2008) is the use of a simple cognitive task, well described in the previous neuroimaging studies and requiring minimum motor responses. While verbal fluency tasks are useful tools for clinical research (Kameyama et al., 2006; Suto et al., 2004; Takizawa et al., 2008), these tasks involve many cognitive processes (e.g., word generation, verbal WM, and cognitive flexibility), making it difficult to characterize what aspects of cognitive processes are indeed relevant to decreased PFC activity associated with negative moods. Our study provides clearer evidence that the PFC is involved in the interaction between naturalistic mood and verbal WM.

We found a significant correlation between mood and PFC activity only for the verbal WM task but not for the spatial WM task. This result could imply that the relationship between mood and PFC activity differs across cognitive functions. Interestingly, some studies have reported that positive and negative moods are differently linked with verbal and spatial cognitive functions (Bartolic et al., 1999; Papousek et al., 2009). In these studies, performances on verbal fluency tasks were relatively worse than those on non-verbal (figural) fluency tasks in negative (dysphoric or withdrawal-related) moods, but opposite in positive (euphoric or approach-related) moods. These results are consistent with our results that showed the negative correlation between negative mood and PFC activity (as well as the trend of positive correlation between positive mood and PFC activity) if we interpret that higher PFC activity corresponds to better cognitive function (see Supplementary Fig. S2). Other studies using WM tasks also showed that verbal and spatial WM functions are selectively associated with experimentally induced positive or negative moods (Gray, 2001; Gray et al., 2002; Shackman et al., 2006). Considering these studies, our results suggest a specific interaction between negative mood and verbal WM under everyday circumstances.

Although the previous studies reported the selective association of mood with spatial WM in an opposite manner to that with verbal WM (Bartolic et al., 1999; Gray, 2001), we did not observed a significant relationship between mood and PFC activity for the spatial WM task. One possibility causing this result is the individual variations in strategy use during the spatial WM task. In the verbal WM task, we used different Japanese morphograms (i.e., Hiragana/Katakana) for target (S1) and probe (S2) stimuli to prompt participants to use a verbal-phonological strategy rather than a visuospatial strategy (Smith et al., 1996). However, the spatial WM task used in our study allowed participants to use either a verbal or spatial strategy because the location of the target stimuli can be remembered by verbal labels (e.g., a number corresponding to each location), as discussed in previous studies (Nystrom et al., 2000). Cortical recruitment during WM tasks is known to depend on strategy use (Glabus et al., 2003). Thus, the homogeneity of strategy use (verbal or spatial) across participants conceivably made the relationship between mood and PFC activity unclear for the spatial WM task. One potential solution is to control the strategy use across participants in future research by using different task paradigms or by providing explicit instructions for memory strategy.

The underlying neural mechanisms of the selective interaction between mood and cognition are still unclear. Some researchers have proposed a "prefrontal asymmetry" hypothesis (Gray, 2001; Gray et al., 2002; Shackman et al., 2006). This hypothesis argues that positive (approach-related) and negative (withdrawal-related) affects are predominantly associated with the left and right hemispheres, respectively, whereby different affects are selectively related to cognitive functions linked with each hemisphere (e.g., verbal-left and spatial-right). However, incorporating our results with this hypothesis is difficult because we did not find clear evidence suggesting hemispheric asymmetry. Another account of the selective interaction between mood and cognition is based on pharmacological evidence. Animal studies have shown that certain cognitive functions involving the PFC (e.g., attentional set-shifting and reversal learning) are distinctly controlled by different neurotransmitters such as dopamine and serotonin (Robbins and Roberts, 2007). Because dopamine and serotonin have been suggested to be associated with positive and negative moods (Mitchell and Phillips, 2007), these transmitters could intermediate the selective interaction between moods and cognitive functions.

It should be noted that previous findings concerning the difference in mood-cognition interaction across cognitive functions remain inconsistent, possibly resulting from the variances in the task paradigms and the mood induction procedures (Shackman et al., 2006). In addition, we found a small but significant difference in accuracy between the tasks, suggesting slightly higher difficulty in the spatial WM tasks than the verbal WM task. This makes it difficult to interpret why we observed the between-task difference in the relationship between mood and PFC activity. Further investigation is needed to illuminate the possible difference between verbal and spatial WM in relation to mood under natural circumstances.

4.3. Limitations

Although we showed that the correlation between negative mood and the PFC activity during the verbal WM task was significant after controlling for age, gender, and task performance, several other factors could still mediate the relationship between mood and PFC activity. For example, this study did not assess or control participants' intelligence. Measures such as intelligence quotient (IQ) or fluid intelligence (gF) are known to be associated with both mood states and PFC activity during WM tasks (Gray et al., 2003; Samuel, 1980). These studies have shown that higher IQ is associated with lower negative moods and that greater gF is associated with more PFC activation during WM tasks. Thus, our results could imply that higher intelligence mediates an inverse relationship between negative moods and PFC activation during the verbal WM task. Another concern is the relationship between naturalistic moods and personality traits. The experimental framework of the present study (i.e., individual-differences approach) precludes us from determining whether the observed relationship between mood and PFC activity derived from state-dependent factors (day-to-day fluctuations in mood states within an individual) or trait-like factors ('*dispositional moods*' persistent across time). Although the POMS questionnaire we used to evaluate the participants' naturalistic moods is considered to evaluate the responders' typical mood states rather than their personality traits (McNair and Heuchert, 2003), the participants' naturalistic moods under their current life situations may depend on their personality traits (Davidson, 2004; Kosslyn et al., 2002). This does not contradict previous fMRI studies suggesting the link between personality traits and PFC activity in response to WM tasks (DeYoung et al., 2009; Kumari et al., 2004). Meanwhile, several experiments have indicated that mood changes within individuals are indeed associated with PFC activity during cognitive tasks (Harrison et al., 2009; Liston et al., 2009). Thus, state-dependent mood factors apart from individual trait factors might at least in part have contributed to our results. To dissociate the contributions of state and trait factors to PFC activity, we need to administer multiple questionnaires for both state and trait measurement (Canli et al., 2004) or to use a within-subject design in which the PFC activity of individual participants is measured over multiple occasions.

5. Conclusion

Our study demonstrated that naturalistic moods in healthy people are related to PFC activity during a verbal WM task. We showed that this relationship remained significant even after controlling for potential confounding factors such as age, gender, and task performance. One thing of note is that a mild variation of naturalistic negative moods among healthy people can be associated with PFC activity even absent experimental affective modulation. The relationship between negative mood and verbal WM in the PFC is particularly of interest, considering clinical findings showing PFC impairment during verbal WM tasks in mood disorders such as major depression (Harvey et al., 2005; Matsuo et al., 2007; Siegle et al., 2007). Further research will lead to more comprehensive understanding of the mood-cognition interaction under broader contexts, bridging the gap across induced moods and naturalistic moods among healthy people, as well as pathological moods in patients with mood disorders.

Acknowledgments

We thank Dr. Akiko Obata and Dr. Hiroaki Kawamichi for their helpful assistance. We also thank Dr. Kisou Kubota for the meaningful discussions we had with him.

Appendix A. Supplementary data

Supplementary data associated with this article can be found, in the online version, at doi:10.1016/j.neures.2011.02.011.

References

Anticevic, A., Repovs, G., Barch, D.M., 2010. Resisting emotional interference: brain regions facilitating working memory performance during negative distraction. Cogn. Affect. Behav. Neurosci. 10, 159–173.

Ashby, F.G., Isen, A.M., Turken, A.U., 1999. A neuropsychological theory of positive affect and its influence on cognition. Psychol. Rev. 106, 529–550.

Baddeley, A., 2003. Working memory: looking back and looking forward. Nat. Rev. Neurosci. 4, 829–839.

Bartolic, E.I., Basso, M.R., Schefft, B.K., Glauser, T., Titanic-Schefft, M., 1999. Effects of experimentally-induced emotional states on frontal lobe cognitive task performance. Neuropsychologia 37, 677–683.
Canli, T., Amin, Z., Haas, B., Omura, K., Constable, R.T., 2004. A double dissociation between mood states and personality traits in the anterior cingulate. Behav. Neurosci. 118, 897–904.
Davidson, R.J., 2004. Well-being and affective style: neural substrates and biobehavioural correlates. Philos. Trans. R. Soc. Lond. B Biol. Sci. 359, 1395–1411.
DeYoung, C.G., Shamosh, N.A., Green, A.E., Braver, T.S., Gray, J.R., 2009. Intellect as distinct from Openness: differences revealed by fMRI of working memory. J. Pers. Soc. Psychol. 97, 883–892.
Eriksen, B.A., Eriksen, C.W., 1974. Effects of noise letters upon the identification of a target letter in a nonsearch task. Percept. Psychophys. 16, 143–149.
Glabus, M.F., Horwitz, B., Holt, J.L., Kohn, P.D., Gerton, B.K., Callicott, J.H., Meyer-Lindenberg, A., Berman, K.F., 2003. Interindividual differences in functional interactions among prefrontal, parietal and parahippocampal regions during working memory. Cereb. Cortex 13, 1352–1361.
Gray, J.R., 2001. Emotional modulation of cognitive control: approach-withdrawal states double-dissociate spatial from verbal two-back task performance. J. Exp. Psychol. Gen. 130, 436–452.
Gray, J.R., Braver, T.S., Raichle, M.E., 2002. Integration of emotion and cognition in the lateral prefrontal cortex. Proc. Natl. Acad. Sci. U.S.A. 99, 4115–4120.
Gray, J.R., Chabris, C.F., Braver, T.S., 2003. Neural mechanisms of general fluid intelligence. Nat. Neurosci. 6, 316–322.
Harrison, N.A., Brydon, L., Walker, C., Gray, M.A., Steptoe, A., Dolan, R.J., Critchley, H.D., 2009. Neural origins of human sickness in interoceptive responses to inflammation. Biol. Psychiatry 66, 415–422.
Harvey, P.O., Fossati, P., Pochon, J.B., Levy, R., Lebastard, G., Lehericy, S., Allilaire, J.F., Dubois, B., 2005. Cognitive control and brain resources in major depression: an fMRI study using the n-back task. NeuroImage 26, 860–869.
Herrmann, M.J., Walter, A., Schreppel, T., Ehlis, A.C., Pauli, P., Lesch, K.P., Fallgatter, A.J., 2007. D4 receptor gene variation modulates activation of prefrontal cortex during working memory. Eur. J. Neurosci. 26, 2713–2718.
Hoshi, Y., Tsou, B.H., Billock, V.A., Tanosaki, M., Iguchi, Y., Shimada, M., Shinba, T., Yamada, Y., Oda, I., 2003. Spatiotemporal characteristics of hemodynamic changes in the human lateral prefrontal cortex during working memory tasks. NeuroImage 20, 1493–1504.
Kameyama, M., Fukuda, M., Yamagishi, Y., Sato, T., Uehara, T., Ito, M., Suto, T., Mikuni, M., 2006. Frontal lobe function in bipolar disorder: a multichannel near-infrared spectroscopy study. NeuroImage 29, 172–184.
Kosslyn, S.M., Cacioppo, J.T., Davidson, R.J., Hugdahl, K., Lovallo, W.R., Spiegel, D., Rose, R., 2002. Bridging psychology and biology. The analysis of individuals in groups. Am. Psychol. 57, 341–351.
Kumari, V., ffytche, D.H., Williams, S.C., Gray, J.A., 2004. Personality predicts brain responses to cognitive demands. J. Neurosci. 24, 10636–10641.
Liston, C., McEwen, B.S., Casey, B.J., 2009. Psychosocial stress reversibly disrupts prefrontal processing and attentional control. Proc. Natl. Acad. Sci. U.S.A. 106, 912–917.
Luciana, M., Collins, P.F., Depue, R.A., 1998. Opposing roles for dopamine and serotonin in the modulation of human spatial working memory functions. Cereb. Cortex 8, 218–226.
Maki, A., Yamashita, Y., Ito, Y., Watanabe, E., Mayanagi, Y., Koizumi, H., 1995. Spatial and temporal analysis of human motor activity using noninvasive NIR topography. Med. Phys. 22, 1997–2005.
Martin, M., 1990. On the induction of mood. Clin. Psychol. Rev. 10, 669–697.
Matsuo, K., Glahn, D.C., Peluso, M.A., Hatch, J.P., Monkul, E.S., Najt, P., Sanches, M., Zamarripa, F., Li, J., Lancaster, J.L., Fox, P.T., Gao, J.H., Soares, J.C., 2007. Prefrontal hyperactivation during working memory task in untreated individuals with major depressive disorder. Mol. Psychiatry 12, 158–166.
Mayer, J.D., McCormick, L.J., Strong, S.E., 1995. Mood-congruent memory and natural mood: new evidence. Pers. Soc. Psychol. Bull. 21, 736–746.
McNair, D.M., Heuchert, J.P., 2003. Profile of Mood States Technical Update. Multi-Health Systems, New York.
McNair, P.M., Lorr, M., Droppleman, L.F., 1971. Profile of Mood States Manual. Educational and Industrial Testing Service, San Diego.
Minagawa-Kawai, Y., van der Lely, H., Ramus, F., Sato, Y., Mazuka, R., Dupoux, E., 2011. Optical brain imaging reveals general auditory and language-specific processing in early infant development. Cereb. Cortex 21, 254–261.
Mitchell, R.L., Phillips, L.H., 2007. The psychological, neurochemical and functional neuroanatomical mediators of the effects of positive and negative mood on executive functions. Neuropsychologia 45, 617–629.
Nystrom, L.E., Braver, T.S., Sabb, F.W., Delgado, M.R., Noll, D.C., Cohen, J.D., 2000. Working memory for letters, shapes, and locations: fMRI evidence against stimulus-based regional organization in human prefrontal cortex. NeuroImage 11, 424–446.
Okamoto, M., Dan, I., 2005. Automated cortical projection of head-surface locations for transcranial functional brain mapping. NeuroImage 26, 18–28.
Oldfield, R.C., 1971. The assessment and analysis of handedness: the Edinburgh inventory. Neuropsychologia 9, 97–113.
Orihuela-Espina, F., Leff, D.R., James, D.R., Darzi, A.W., Yang, G.Z., 2010. Quality control and assurance in functional near infrared spectroscopy (fNIRS) experimentation. Phys. Med. Biol. 55, 3701–3724.
Papousek, I., Schulter, G., Lang, B., 2009. Effects of emotionally contagious films on changes in hemisphere-specific cognitive performance. Emotion 9, 510–519.
Parrot, W.G., Sabini, J., 1990. Mood and memory under natural conditions: evidence for mood incongruent recall. J. Pers. Soc. Psychol. 59, 321–336.
Pena, M., Maki, A., Kovacic, D., Dehaene-Lambertz, G., Koizumi, H., Bouquet, F., Mehler, J., 2003. Sounds and silence: an optical topography study of language recognition at birth. Proc. Natl. Acad. Sci. U.S.A. 100, 11702–11705.
Perlstein, W.M., Elbert, T., Stenger, V.A., 2002. Dissociation in human prefrontal cortex of affective influences on working memory-related activity. Proc. Natl. Acad. Sci. U.S.A. 99, 1736–1741.
Qin, S., Hermans, E.J., van Marle, H.J., Luo, J., Fernandez, G., 2009. Acute psychological stress reduces working memory-related activity in the dorsolateral prefrontal cortex. Biol. Psychiatry 66, 25–32.
Robbins, T.W., Roberts, A.C., 2007. Differential regulation of fronto-executive function by the monoamines and acetylcholine. Cereb. Cortex 17, i151–i160.
Robinson, O.J., Sahakian, B.J., 2009. A double dissociation in the roles of serotonin and mood in healthy subjects. Biol. Psychiatry 65, 89–92.
Samuel, W., 1980. Mood and personality correlates of IQ by race and sex of subject. J. Pers. Soc. Psychol. 38, 993–1004.
Sato, H., Fuchino, Y., Kiguchi, M., Katura, T., Maki, A., Yoro, T., Koizumi, H., 2005. Inter-subject variability of near-infrared spectroscopy signals during sensorimotor cortex activation. J. Biomed. Opt. 10, 44001.
Sato, H., Takeuchi, T., Sakai, K.L., 1999. Temporal cortex activation during speech recognition: an optical topography study. Cognition 73, B55–B66.
Schroeter, M.L., Zysset, S., Wahl, M., von Cramon, D.Y., 2004. Prefrontal activation due to Stroop interference increases during development–an event-related fNIRS study. NeuroImage 23, 1317–1325.
Shackman, A.J., Sarinopoulos, I., Maxwell, J.S., Pizzagalli, D.A., Lavric, A., Davidson, R.J., 2006. Anxiety selectively disrupts visuospatial working memory. Emotion 6, 40–61.
Siegle, G.J., Thompson, W., Carter, C.S., Steinhauer, S.R., Thase, M.E., 2007. Increased amygdala and decreased dorsolateral prefrontal BOLD responses in unipolar depression: related and independent features. Biol. Psychiatry 61, 198–209.
Singh, A.K., Dan, I., 2006. Exploring the false discovery rate in multichannel NIRS. NeuroImage 33, 542–549.
Singh, A.K., Okamoto, M., Dan, H., Jurcak, V., Dan, I., 2005. Spatial registration of multichannel multi-subject fNIRS data to MNI space without MRI. NeuroImage 27, 842–851.
Smith, E.E., Jonides, J., 1999. Storage and executive processes in the frontal lobes. Science 283, 1657–1661.
Smith, E.E., Jonides, J., Koeppe, R.A., 1996. Dissociating verbal and spatial working memory using PET. Cereb. Cortex 6, 11–20.
Suda, M., Fukuda, M., Sato, T., Iwata, S., Song, M., Kameyama, M., Mikuni, M., 2009. Subjective feeling of psychological fatigue is related to decreased reactivity in ventrolateral prefrontal cortex. Brain Res. 1252, 152–160.
Suda, M., Sato, T., Kameyama, M., Ito, M., Suto, T., Yamagishi, Y., Uehara, T., Fukuda, M., Mikuni, M., 2008. Decreased cortical reactivity underlies subjective daytime light sleepiness in healthy subjects: a multichannel near-infrared spectroscopy study. Neurosci. Res. 60, 319–326.
Suto, T., Fukuda, M., Ito, M., Uehara, T., Mikuni, M., 2004. Multichannel near-infrared spectroscopy in depression and schizophrenia: cognitive brain activation study. Biol. Psychiatry 55, 501–511.
Takizawa, R., Kasai, K., Kawakubo, Y., Marumo, K., Kawasaki, S., Yamasue, H., Fukuda, M., 2008. Reduced frontopolar activation during verbal fluency task in schizophrenia: a multi-channel near-infrared spectroscopy study. Schizophr. Res. 99, 250–262.
Tsujimoto, S., Yamamoto, T., Kawaguchi, H., Koizumi, H., Sawaguchi, T., 2004. Prefrontal cortical activation associated with working memory in adults and preschool children: an event-related optical topography study. Cereb. Cortex 14, 703–712.
Yokoyama, K., Araki, S., Kawakami, N., Takeshita, T., 1990. Production of the Japanese edition of profile of mood states (POMS): assessment of reliability and validity. Nippon Koshu Eisei Zasshi 37, 913–918.

Chapter 12
Fabrication of Growth Factor Array Using an Inkjet Printer

Kohei Watanabe, Tomoyo Fujiyama, Rina Mitsutake, Masaya Watanabe, Yukiko Tazaki, Takeshi Miyazaki, and Ryoichi Matsuda

Abstract Although multiple growth factors influence the fate of cells in vivo, it is technically difficult to reproduce similar condition in vitro. To overcome this problem, we have developed growth factor array, a system to study compound effects of multiple growth factors fabricated with a commercial color inkjet printer. By replacing color inks to 2–4 growth factors and printing them on the tissue culture substratum, we prepared growth factor arrays. Culturing cells on the array, we studied the compound effects of growth factors during myogenic and/or osteogenic differentiation of C2C12 myoblast and mesenchymal stem cells in a single culture dish. The cells grown on the array exhibited various levels of differentiation depending on the dose and the combination of growth factors. Since inkjet printer is capable to manipulate several colors simultaneously, this method is suitable for multivariate analyses of growth factors. This method may provide a powerful tool for regenerative medicine, especially for stem cell research on the control of cell-fate determination and differentiation.

12.1 Introduction

In living organisms, cells are constantly under the influence of extrinsic environmental factors such as growth factors, hormones, and extracellular matrices. Proliferation, differentiation, migration, and cell death are controlled by a complicated combination of stimuli from these factors. The mechanisms of these factors in the developmental processes of multi-cellular organisms have not yet been clarified completely, potentially due to the enormous number of factors that have to be examined in order to construct the in vivo conditions in vitro. Conventional studies

K. Watanabe (✉)
Department of Life Sciences, The University of Tokyo, Tokyo 153-8902, Japan; Canon Inc., Tokyo 146-8501, Japan
e-mail: watanabe.kohei@canon.co.jp

B.R. Ringeisen et al. (eds.), *Cell and Organ Printing*,
DOI 10.1007/978-90-481-9145-1_12, © Springer Science+Business Media B.V. 2010

with simple experimental systems considering one or two factors give insufficient analytical results.

Researches are actively pursuing methods to convert these stem cells into specific cell types to supplement damaged tissues. For example, it has been reported that marrow stromal cells can differentiate to adipocytes, chondroblasts, osteoblasts, cardiac muscle cells, hepatocytes, and neurons under certain culture conditions [1, 2, 3, 4]. Furthermore, muscle satellite cells, which are usually in quiescent state and activated for muscle regeneration process, can also differentiate to adipocytes, osteocytes, and chondrocytes by treating them with certain growth factors. Undifferentiated mouse embryonic stem (ES) cells have been found to express FGF receptor FGFR1, -R2, and -R3 [5]. The expression of IGF-1 receptors in C3H10T1/2 fibroblast is stimulated by BMP-2 [47]. As exemplified above, multiple receptors are expressed in one cell, suggesting that the stimulations from multiple factors may lead to novel effects which were not yet identified. Avila et al. [6] reported that neural differentiation of PC12 pheochromocytoma cell line was promoted by the presence of nicotine and nerve growth factor (NGF). Zebboudj et al. [7] reported that coexistence of matrix GLA protein and bone morphogenetic protein-2 (BMP-2) promotes calcification of blood vessels. Myogenic differentiation of C2C12 myoblast cell line was enhanced by IGF-I but inhibited by FGF-2 [8]. Furthermore, C2C12 muscle cells exhibit osteogenic differentiation by BMP-2 and IGF-I [9, 10]. All these reports suggest that experiments using a combination of multiple factors, not a single factor, at a wide range of concentrations is necessary.

It has been shown that no single growth factor is sufficient for deciding the differentiation fate of ES cells. Schuldiner et al. [11] examined eight different growth factors for human ES cells and reported that none of these directed differentiation to only one cell type, but, rather, altered the relative populations of a specific cell type. Loeser et al. [12] reported that coexistence of insulin-like growth factor-I (IGF-I) and bone morphogenetic protein 7 (BMP-7) stimulates the growth of chondrocytes. Although activin A induces various cell types in amphibian embryonic cells, it is not sufficient to induce phenotypes in murine ES cells [13, 14]. Therefore, the tools for analyzing the compound effect of multiple factors will make it possible to find the optimum conditions for cell differentiation efficiently.

In recent years, computer-aided tissue engineering technology called 'bioprinting' has emerged [15]. Inkjet technology has drawn attention as a powerful tool for biological research [16]. Inkjet technology is capable of ejecting solutions evenly in any place or area, enabling easy preparation of computer-generated patterns on the substratum. Since inkjet printers can eject tiny droplets at the picoliter scale, it is possible to easily control the amount of deposited substance by changing the number of ejections at any one place. Exploiting this characteristic, studies in DNA microarray preparation [17, 18, 19], protein handling [20, 21], and patterning of cells [22–24] have been reported. Furthermore, inkjet technology can be also used for analyzing the compound effects of multiple factors. We have previously proposed the concept of 'Growth Factor Array', a novel cell-based analysis tool. Growth factor arrays are fabricated with a conventional color inkjet

printer by replacing color inks to solutions containing growth factors and printing them on the tissue culture substratum [25]. Since growth factor arrays make it possible to analyze compound effects of multiple growth factors on single culture dish, it can be used to analyze the optimal conditions for differentiation of stem cells. This idea has been adopted by other research groups [26, 27].

In this chapter, we present our work on growth factor array fabrication, giving several experimental examples to prove the concept of the growth factor array. Growth factor arrays composed of 2–4 growth factors were fabricated with several approaches for growth factor immobilization onto the substratum.

12.2 Materials and Methods

12.2.1 Materials

Fibroblast Growth Factor-2 (FGF-2), Insulin-like Growth Factor-I (IGF-I), Bone Morphogenetic Protein-2 (BMP-2), Epidermal Growth Factor (EGF), Platelet-derived growth factor-BB (PDGF-BB) were purchased from R&D Systems Inc. (Minnesota, USA). [^{125}I] IGF-I and horseradish peroxidase conjugated anti-mouse IgG antibody were purchased from Amersham Biosciences Corp (New Jersey, USA). Alexa Fluoro 488 conjugated anti-rabbit IgG antibody, Alexa Fluoro 680 conjugated anti-mouse IgG antibody, and TOTO-3 were purchased from Molecular Probes, Inc. (Oregon, USA). Anti-myogenin polyclonal antibody was purchased from Santa Cruz Biotechnology. MF20 hybridoma was purchased from Developmental Studies Hybridoma Bank (Univ. Glowa), and its culture supernatant was used as the anti-mouse striated muscle type myocin heavy chain (MyHC) antibody. Anti-alkaline phosphatase monoclonal antibody was purchased from Biogenesis Ltd. (Poole, UK). IRDye 800 conjugated anti-mouse IgG antibody was purchased from Rockland Immunochemicals, Inc. (Pennsylvania, USA).

Dulbecco's Modified Eagle's Medium (DMEM) -high glucose type, fetal bovine serum (FBS), Antibiotic-Antimicotic, trypsin-EDTA, bovine insulin, and holo-transferrin were purchased from Invitrogen Corp. (California, USA). Bovine fibronectin was purchased from Itoham Foods Inc. (Hyogo, Japan). Other reagents were purchased from SIGMA-Aldrich, unless otherwise noted.

Inkjet printers used in this research were BJ F850, PIXUS 950i, Pixus iP8600 (all from Canon, Tokyo Japan). They were used with some modification, as described in the following sections.

Mouse myoblast cell line C2C12 was kindly provided from Dr. Yoichi Nabeshima of National Center of Neurology and Psychiatry, Japan. For C2C12 cell culture, DMEM containing 20% FBS was used as growth medium. As the differentiation medium, DMEM containing 10 μg/mL insulin, 5 μg/mL transferrin, 5 nM sodium selenite, 1 mg/mL bovine serum albumin (ITS medium) or DMEM containing 2% FBS was used.

12.2.2 Growth Factor Array Using Photoreactive Growth Factors

Growth factor arrays using photoreactive growth factors were prepared as described below. Photoreactive IGF-I, FGF-2, [^{125}I] IGF-I were prepared by introducing a phenyl azide group to growth factors, according to the methods described in previous works [28, 29]. The cover of the inkjet printer BJ F850 was removed, and the print head was washed with distilled water. Polystyrene substratum was placed 1 mm beneath the print head. Photoreactive growth factors were injected into the print head, and the growth factors were printed onto the substratum. To increase the density of the growth factor in a certain area, the number of printed droplets in that area was multiplied. After the printing, substratum was UV-irradiated at a distance of 10 cm for 20 s using a mercury lamp (Zeiss HBO 50, 50 W) to immobilize the growth factor on the substratum. Residual growth factors were removed by washing with PBS. With this method, a bifactor growth factor array with 16 areas representing combinations of IGF-I and FGF-2 at various concentrations was prepared. To examine the fidelity of printing and the efficiency of growth factor immobilization at each stage of this process, photoreactive [^{125}I] IGF-I was prepared and evaluated by measuring the γ-ray intensity.

For growth factor array analysis, C2C12 myoblasts were inoculated at 50 cells/mm^2 in growth medium, and after 24 h the medium was replaced with ITS-medium as differentiation medium. After a further 24 h of culture, cells were fixed with methanol, and immunostained with anti-myogenin antibody as a marker of myogenic differentiation. Anti-rabbit IgG-Alexa Fluor 488-labeled antibody was used as the secondary antibody. Nuclear DNA was also stained with Hoechst 33258. For comparison with the effect of growth factors in soluble state, combinations of IGF-I and FGF-2 in soluble state were examined at concentrations of 0, 2, 8 and 20 ng/mL, resulting in 16 combinations.

12.2.3 Growth Factor Array with Surface Activated Substratum

Substrata with activated surface to immobilize growth factors were prepared by treating the surface of the substrata with tresyl activated dextran according to the previous method [30]. Growth factors dissolved in carbonate buffer (pH 7.2) containing 0.3% glycerin were printed with inkjet printer Pixus 950i on the surface activated substratum. The substratum was incubated at 4°C for 16 h in moist conditions. Residual growth factors were removed by washing with PBS, and the remaining active groups were blocked with 0.1% gelatin or fibronectin solution. By this method, growth factor arrays composed of 3 growth factors (IGF-I, FGF-2, BMP-2) (Fig. 12.1) and 4 growth factors (IGF-I, FGF-2, BMP-2, PDGF) were prepared. The efficiency of growth factor immobilization on the surface activated substratum was extrapolated from the measured efficiency of immobilization of BSA.

For growth factor array analysis, C2C12 cells were cultured in growth medium for 24 h followed by the medium replacement with the differentiation medium containing 2% FBS. After 4 days cells were fixed with 10% formalin, blocked for

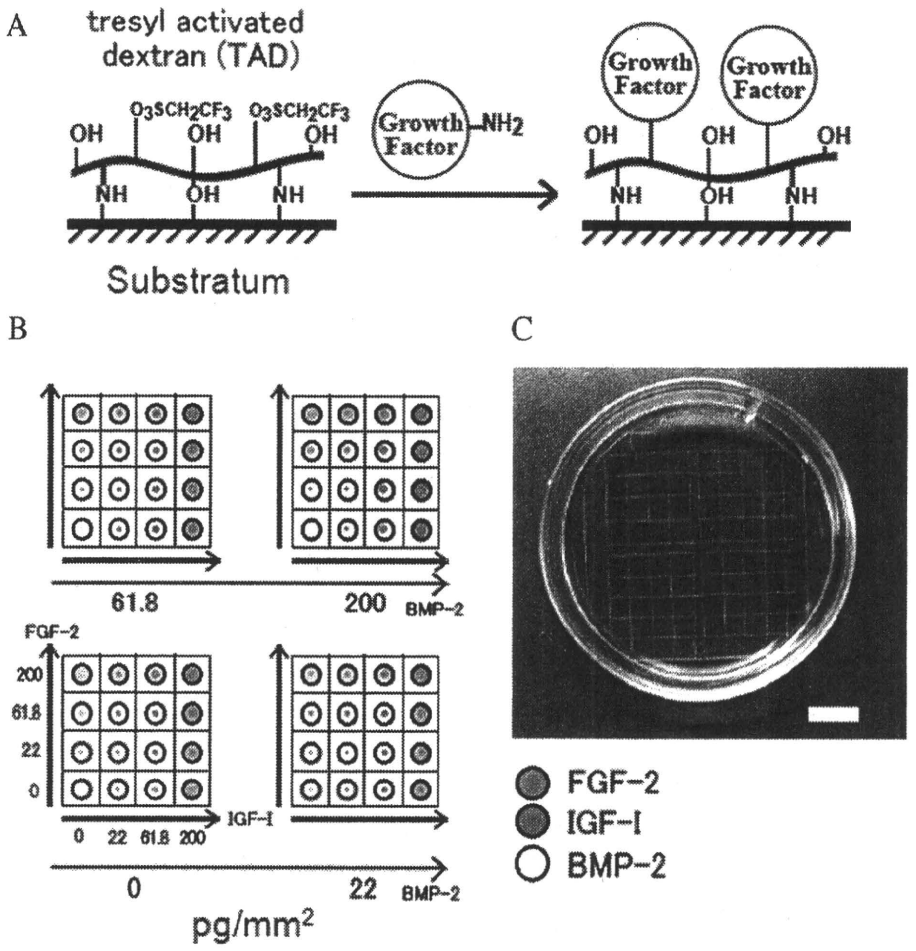

Fig. 12.1 Preparation of growth factor array using surface activated substratum. (**a**) Immobilization of growth factors by TAD-treated substratum. (**b**) Printed patterns of 3 growth factors on the surface activated substratum (pg/mm^2). (**c**) Growth factor array with surface activated substratum placed in a culture dish (scale bar: 1 cm)

1 h, and immunostained with either monoclonal anti-ALP antibody as osteogenic marker or anti-MyHC monoclonal antibody as myogenic marker, and further stained with Anti-mouse IgG IRDye 800-labeled antibody. Cells were also stained with TOTO-3 as the indicator of the cell number. The fluorescent intensity from TOTO-3 and differentiation markers were measured with the fluorescent image analyzer Odyssey (LI-COR).

12.2.4 Growth Factor Array in Liquid System

In order to compare the effects of growth factors on the surface activated substratum with those in the soluble state, growth factor arrays in liquid system were prepared as described below. Solutions of growth factors were dissolved in distilled water containing 5% glycerin. The solutions were printed with Pixus 950i in the pattern that matches the wells of 96-well plate. After printing, 200 μL of differentiation

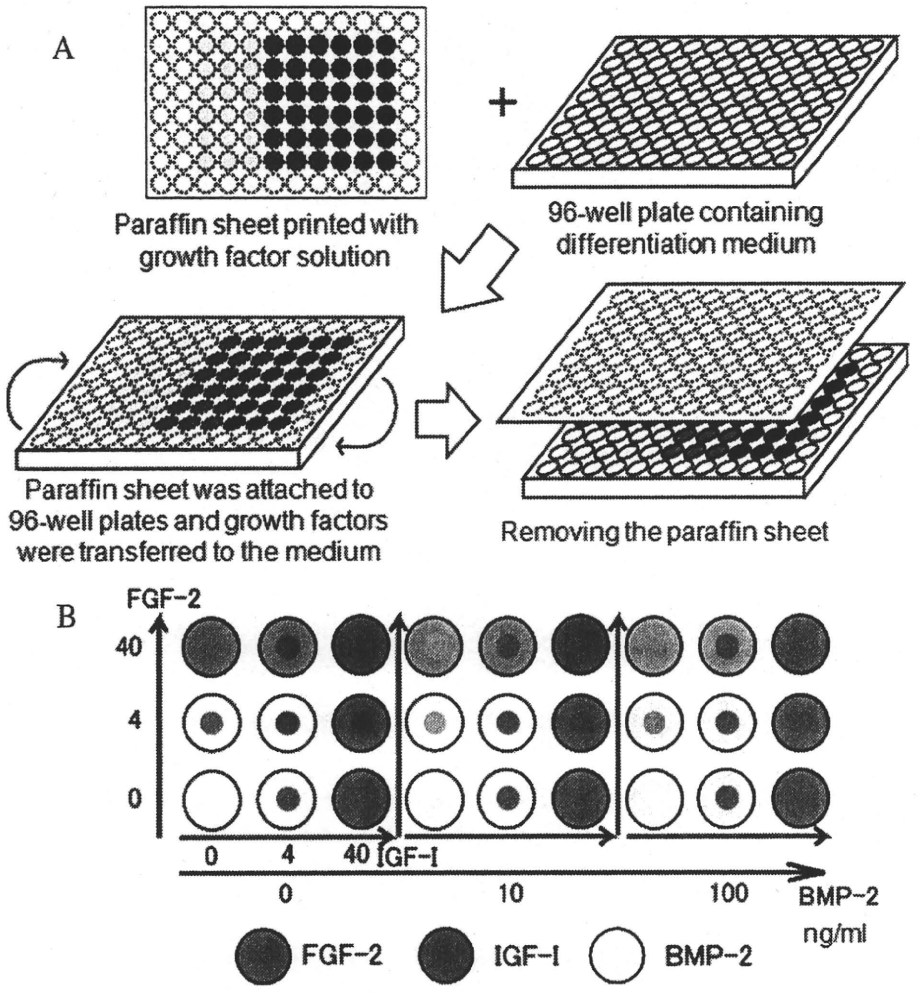

Fig. 12.2 Preparation of growth factor array in liquid system. (**a**) Schematic diagram of preparation of growth factor array in liquid system using paraffin sheets and 96-well plate. (**b**) Printed pattern of 3 growth factors on the paraffin sheets (ng/mL)

medium was injected in the wells of 96-well plates and the sheets were touched tightly to the 96-well plate, so that the printed areas corresponded to the wells. The plate was inverted to dissolve the growth factors in the medium, according to the previous method [31] (Fig. 12.2).

12.2.5 Growth Factor Array with Slow-Release System

Growth factor arrays with slow-release system were prepared as follows. Photoreactive gelatin was prepared by introducing a phenyl azide group to gelatin molecule in the same manner with the photoreactive growth factors. Photoreactive gelatin solution with and without growth factors dissolved in PBS were infused in the print head of inkjet printer iP8600. First, photoreactive gelatin without growth factors was printed on the substratum and air-dried. Then, solution containing growth factors were printed and air-dried. After printing, substratum was

UV-irradiated at an intensity of 20 mJ/cm^2 using a UV-crosslinker, and washed with distilled water 3 times. The total amount of photoreactive gelatin printed in each area was controlled such that the same amount was deposited in all areas. In order to avoid the attachment of cells outside of the printed areas, substrata were coated with graft copolymer of poly-L lysine and polyethylene glycol (PLL-g-PEG) synthesized according to the previous work [32].

To examine the slow-releasing effect of growth factors from the substratum, 96-well plate was incubated with the mixture of photoreactive gelatin and EGF then UV-irradiated at 0.2, 2, 20 and 200 mJ/cm^2. After the UV-irradiation, the wells were incubated with 200 μL of PBS containing 0.1% BSA at 37°C. The supernatant was sampled and the amount of EGF in the supernatant was determined by ELISA.

To examine the feasibility of growth factor array with slow-release system, C2C12 cells in growth medium were suspended in differentiation medium and cultured at 2×10^4 cells/cm^2. After 4 days of culture, the differentiation analysis was performed in the same manner with that of growth factor array with surface activated substratum.

MSCs were also cultured with growth factor arrays in a slow-releasing system as follows. MSCs isolated from the femur of a Wister rat (3 weeks, male) were cultured on the growth factor array with slow-release system at 1×10^4 cells/cm^2 in alphaMEM containing 15% FBS, 10^{-8} M dexamethasone, 10 mM β-glycerophosphate, 50 μg/mL ascorbic acid for 14 days [33]. Medium was changed every 4 days. After 14 days, cells were fixed with 10% formaldehyde and evaluated the bone differentiation by immunostaining with anti-ALP antibody.

12.3 Results

12.3.1 Growth Factor Array with Photoreactive Growth Factors

In order to examine the accuracy of growth factor printing with the inkjet printer and the immobilization rate of photoreactive growth factors, photoreactive [^{125}I] IGF-I was prepared. From the measured intensity of γ-ray from the printed [^{125}I] IGF-I as well as that remaining on the substratum after washing, it turned out that the printing of solutions is accurate and stable, but the immobilization efficiency decreased as the amount of protein increased.

Growth factor arrays consisted of 16 combinations of IGF-I and FGF-2 were prepared. The quantity of immobilized IGF-I and FGF-2 was calculated from the immobilization rate obtained from the previous result are 0, 21, 64, and 149 pg/mm^2 and 0, 41, 79, 175 pg/mm^2, respectively. C2C12 cells were cultured on the growth factor array for 48 hr in growth medium, followed by another 24 hr in differentiation medium. In order to compare the effect of growth factors immobilized on the array with those in a soluble state, C2C12 cells were cultured under 16 different conditions corresponding to combinations of four different concentrations (0, 2, 8, 20 ng/mL) of IGF-I and FGF-2. For both experiments, the onset of myogenin

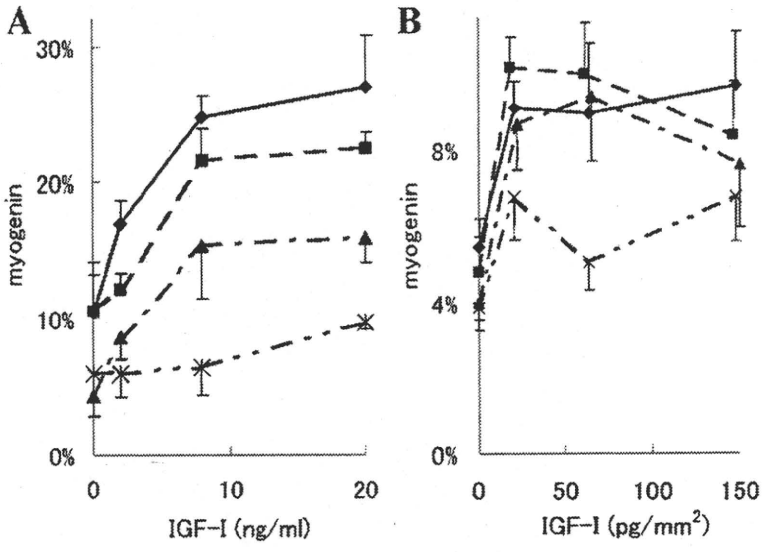

Fig. 12.3 Effect of IGF-I and FGF-2 on myogenin expression. (**a**) C2C12 cells were cultured with soluble IGF-I (0, 2, 8, 20 ng/mL) in combination with soluble FGF-2 (0(□), 2(■), 8(▲), 20(×) ng/mL). (**b**) C2C12 cells were cultured on growth factor arrays containing 16 sections consisting of IGF-I (0, 21, 64, 149 pg/mm^2) and FGF-2 (0(□), 41(■), 79(▲), 175(×) pg/mm^2)

expression was examined. When C2C12 cells were cultured on the growth factor arrays, the myogenin expression ratio varied among the different combinations of IGF-I and FGF-2 (Fig. 12.3). However, the myogenin expression pattern was different from that of the soluble growth factors. For soluble growth factors, the effect of IGF-I was remarkably high at 8 ng/mL and approximately 20 ng/mL of IGF-I appeared to be close to saturation. On the growth factor arrays, the ratio of the myogenin expression increased with 21 pg/mm^2 of IGF-I, though the higher quantity of IGF-I barely increased its stimulation. In contrast, the suppressive effect of FGF-2 was very clear for soluble FGF-2. However, the effect of the FGF-2 immobilized on the growth factor array seemed to be weaker. Only the concentration of 175 pg/mm^2 FGF-2 lowered the myogenin expression ratio.

12.3.2 Growth Factor Array with Surface Activated Substratum

12.3.2.1 Growth Factor Array with 3 Growth Factors

The immobilization efficiency of surface activated substratum was evaluated with BSA by ELIZA. The concentrations of growth factors used in this experiment did not exceed the immobilization capacity of activated surface. Hence, the concentrations of growth factors immobilized on the surface activated substratum were estimated from the printed quantity.

C2C12 cells were cultured on growth factor arrays fabricated with surface activated substratum. These arrays consisted of combinations of printed FGF-2, IGF-I and BMP-2 (0, 22, 61.8, 200 pg/mm^2, respectively) with 64 areas in all. Cell growth

or differentiation was significantly promoted on the areas where growth factors were immobilized.

To analyze the effects of growth factor combinations for myogenic differentiation, the relative fluorescent intensity of MyHC was obtained by standardizing with fluorescent intensity of TOTO-3 (Fig. 12.3). Without BMP-2, MyHC expression increased with IGF-I dose, but this effect was attenuated by FGF-2. However, when BMP-2 co-existed in the area, especially in high concentrations, the attenuation effect by FGF-2 was unstable.

To analyze the effects of growth factor combinations for osteogenic differentiation, the relative fluorescent intensity of ALP was obtained by standardizing fluorescent intensity of TOTO-3, but the relative fluorescent intensity of ALP was weak independent of the presence of BMP-2 (Data not shown).

12.3.2.2 Growth Factor Analysis in Liquid System with 3 Growth Factors

Growth factor arrays in liquid system were prepared to compare with the growth factor arrays fabricated with surface activated substratum. First, 3 growth factors, IGF-I (0, 4, and 40 ng/mL), FGF-2 (0, 4 and 40 ng/mL) and BMP-2 (0, 10 and 100 ng/mL) were used to prepare growth factor array in liquid system, resulting in 27 combinations (Fig. 12.2). After culturing C2C12 myoblast with this growth factor array in liquid system, TOTO-3, MyHC, and ALP were immunostained, and the fluorescent intensity was compared in the same way shown before. Relative fluorescent intensity of MyHC standardized by TOTO-3 fluorescent intensity is shown in Fig. 12.5. Without BMP-2, relative fluorescent intensity of MyHC increased as the concentration of IGF-I increase and this effect was attenuated by FGF-2. When BMP-2 coexists, expression of MyHC was suppressed and the relative fluorescent intensity decreased dose dependently. At high concentration (100 ng/mL) of BMP-2, the activity of IGF-I to promote differentiation to myoblasts was almost completely suppressed.

12.3.2.3 Evaluation of Immobilized BMP-2

Since the effect of immobilized BMP-2 was not clear in previous experiments, the effect of BMP-2 at higher concentrations was evaluated independently. BMP-2 was

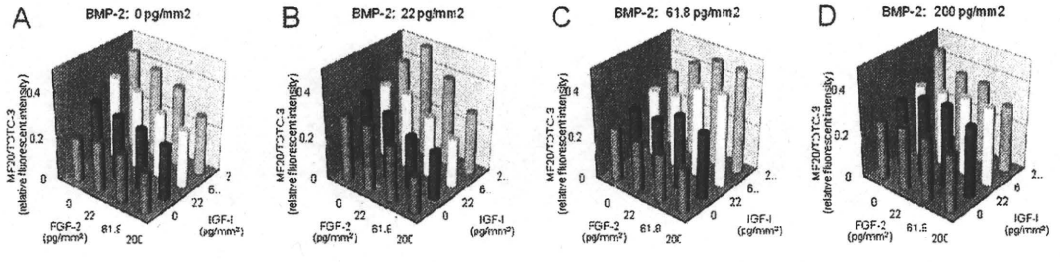

Fig. 12.4 Myogenic differentiation of C2C12 myoblast cultured on the growth factor array fabricated with surface activated substratum. The relative fluorescent intensity of MyHC was obtained by standardizing with fluorescent intensity of TOTO-3

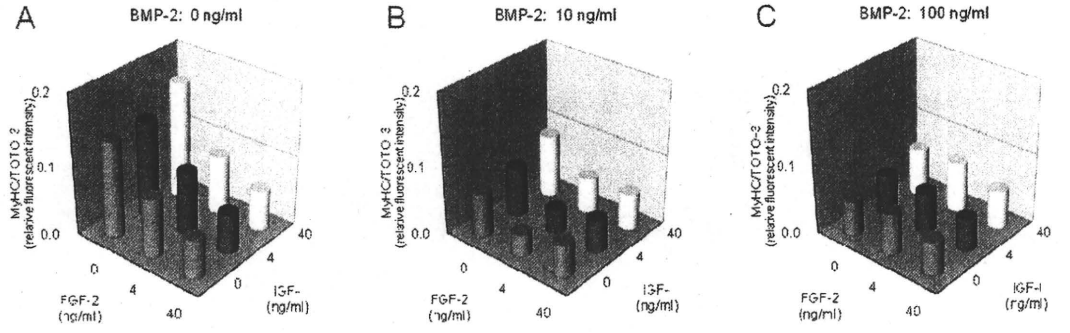

Fig. 12.5 Myogenic differentiation on growth factor array in liquid system consisted of 3 growth factors; IGF-I, FGF-2, and BMP-2. Relative fluorescent intensity of MyHC increased as the concentration of IGF-I increase and this effect was attenuated by FGF-2. When BMP-2 coexists, expression of MyHC was suppressed and the relative fluorescent intensity decreased with dosage

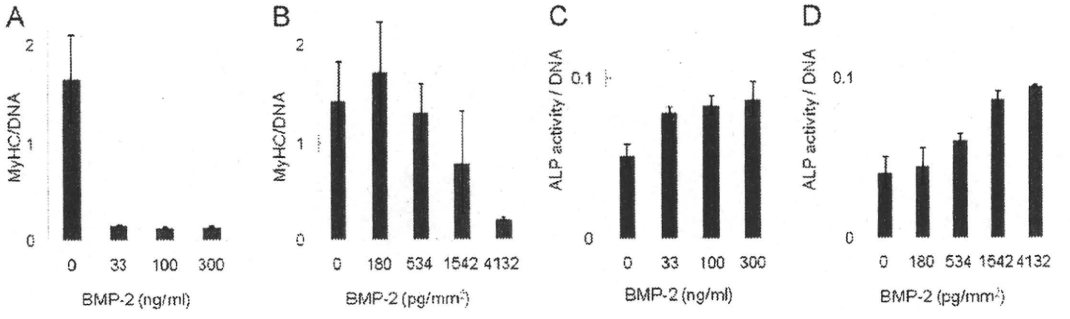

Fig. 12.6 The effect of myogenic differentiation by soluble BMP-2(**a**) and immobilized BMP-2 (**b**) and the effect of osteogenic differentiation by soluble BMP-2 (**c**) and immobilized BMP-2 (**d**)

immobilized on the surface-activated substratum and C2C12 was cultured on that substratum. In this experiments, higher concentration of BMP-2 works inhibitory for MyHC expression and enhanced ALP expression dose dependently, which correspond to the effect of soluble BMP-2 (Fig. 12.6). In this experiment, the highest concentration immobilized on the substratum was 4132 pg/mm^2, corresponding to 536 ng/ml in the soluble state, which is an enormously high concentration compared to the normal experimental condition in vivo or in vitro. At 1542 pg/mm^2, little effect for inhibition for myogenic differentiation was observed, whereas bone differentiation was close to the effect of soluble BMP-2 at 33 ng/ml. These results indicate that the activity of BMP-2 was lowered or changed through the printing and/or immobilization process to the substratum.

12.3.2.4 Growth Factor Array with 4 Growth Factors

Growth factor arrays composed of 4 growth factors were also prepared with surface activated substratum (Fig. 12.7a). This growth factor array consisted of 81 areas with combinations of EGF, FGF-2, IGF-I and PDGF, and the compound effects of these factors were examined. These proteins are known to promote the growth of C2C12 and FGF-2 is inhibitory for myogenic differentiation dose-dependently. C2C12

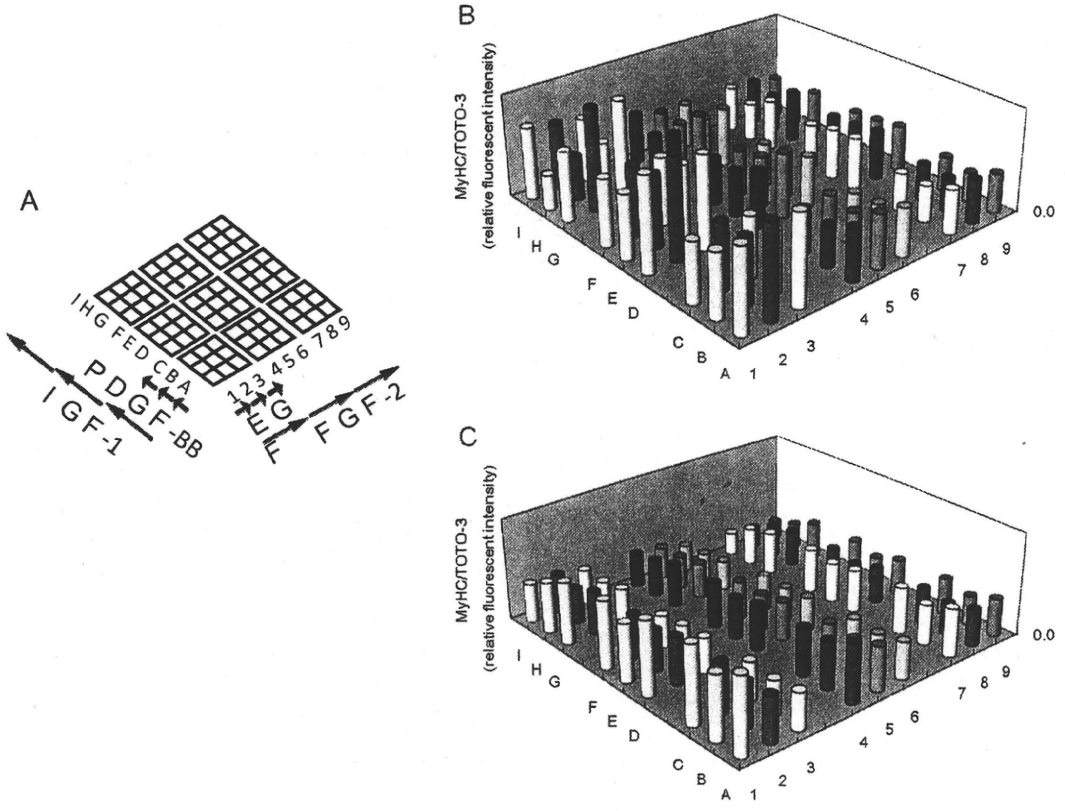

Fig. 12.7 Analysis of 4 growth factors. (**a**) The schematic diagram of growth factor array with 4 growth factors (EGF, PDGF-BB, FGF-2, IGF-I) fabricated with surface activated substratum and that in liquid system. (**b**) The effect of myogenic differentiation analyzed on the growth factor array with 4 growth factors fabricated with surface activated substratum. The concentrations of growth factors are as follows. EGF: 0, 67, 200 pg/mm^2, PDGF-BB: 0, 100, 300 pg/mm^2, FGF-2: 0, 67, 200 pg/mm^2, IGF-I: 0, 133, 400 pg/mm^2. (**c**) Myogenic differentiation on growth factor array in liquid system. The concentrations of growth factors are as follows. EGF: 0, 15, 44 ng/mL, PDGF-BB: 0, 22, 66 ng/mL, FGF-2: 0, 15, 44 ng/mL, IGF-I: 0, 30, 88 ng/mL

myoblasts were cultured on this growth factor array for 8 h in growth medium, then 72 hr in differentiation medium. After the culture, cell growth and myogenic differentiation was analyzed by staining TOTO-3 and MyHC antibody, respectively (Fig. 12.7b). The results show that cell growth was promoted by IGF-I, EGF, and FGF-2 but not by PDGF-BB. The compound effect for cell growth was similar to the sum of the effect of individual growth factors. Myogenic differentiation was inhibited by EGF but not by FGF-2 and PDGF-BB.

12.3.2.5 Growth Factor Array in Liquid System with 4 Growth Factors

Growth factor arrays in a liquid system composed of 4 soluble growth factors were also prepared in the same method. The growth factor pattern is the same as growth factor array in solid system (Fig. 12.7a). As a result, EGF, FGF-2, IGF-1 and PDGF-BB were promotive for growth of C2C12. FGF-2, EGF and PDGF-BB were inhibitory for myogensis (Fig. 12.7c). The inhibitory effect of FGF-2 and EGF was higher than that of immobilized growth factors.

12.3.3 Growth Factor Array with Slow Release System

12.3.3.1 Evaluation of Slow Release of Growth Factors

To evaluate the slow-release of growth factors, EGF was retained on the substrate with photoreactive gelatin with different photo-crosslink conditions. After immobilization of growth factors, the quantity of EGF released to PBS was measured with ELIZA (Fig. 12.8a). EGF release was detected within 24 h at all the conditions. However, when UV-irradiation condition was low (0.2 mJ/cm^2) or high (200 mJ/cm^2), the amount of EGF in PBS was constant while EGF amount increased at intermediate condition of UV irradiation (2 and 20 mJ/cm^2). After 7 days, EGF on the substratum was immunostained with anti-EGF antibody (Fig. 12.8b). Little EGF was detected with the substratum irradiated with 0.2 and 2 mJ/cm^2 UV, while retained EGF was still detected at the substratum irradiated with 20 and 200 mJ/cm^2. According to this result, the remaining experiments were operated with a 20 mJ/cm^2 UV-irradiation.

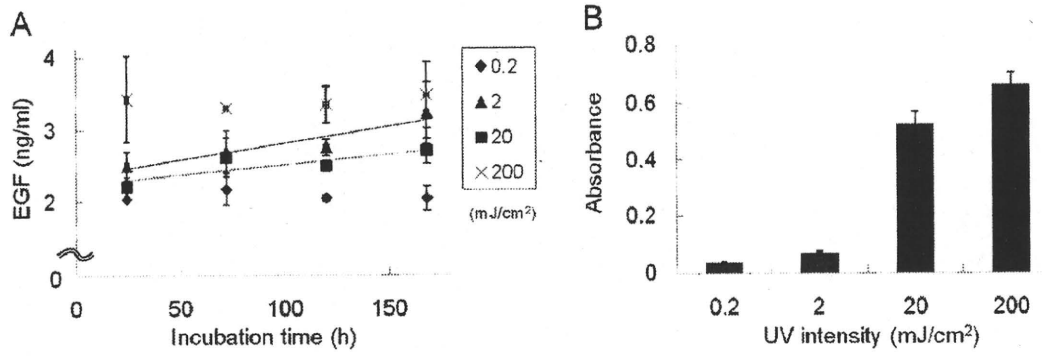

Fig. 12.8 Evaluation of slow-release of growth factors. (**a**) The quantity of released growth factor from the substratum was measured by detecting the released EGF in PBS by ELIZA. (**b**) Remaining EGF on the substratum after 7 days incubation in PBS detected by immunostaining the substratum with EGF antibody

12.3.3.2 Culture of C2C12 Myoblast with Growth Factor Array in Slow Release System

C2C12 myoblast was cultured on the growth factor arrays with slow release system consisting of IGF-I and BMP-2. After the culture, C2C12 was immunostained with TOTO-3 and either with anti-MyHC antibody as a myogenic marker or anti-ALP antibody as an osteogenic marker (Fig. 12.9). Cell growth was not significantly different among each area. However, myogenic differentiation was suppressed by BMP-2 in a dose-dependent manner. At the highest concentration of BMP-2 (450 pg/mm^2), even the effect of myogenic differentiation by IGF-I was completely suppressed. On the contrary, osteogenic markers were not significantly different among areas (Data not shown).

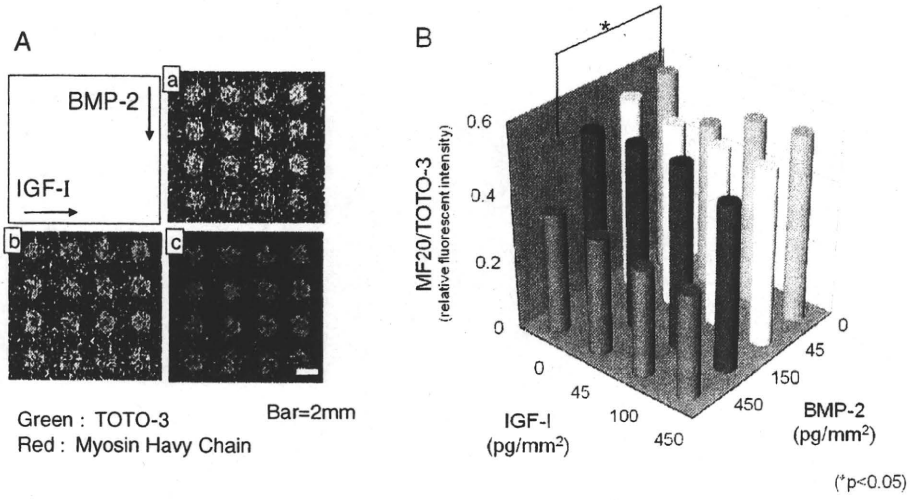

Fig. 12.9 Effect of BMP-2 and IGF-I on C2C12 culture in growth factor array with slow-release system. (**a**) C2C12 myoblast was cultured for 4 days on growth factor array in slow-release system. **a**: Merge, **b**: Fluorescence image of TOTO-3 staining. c: Fluorescence image indicating myogenic differentiation (scale bar: 2 mm). (**b**) Cells were immunostained with anti-MyHC antibody. Relative intensity of MF20 was measured. At the highest concentration of BMP-2(450 pg/mm^2), even the effect of myogenic differentiation by IGF-I was completely suppressed

12.3.3.3 MSC Culture on Growth Factor Array with Slow Release System

MSCs were cultured on the growth factor arrays with slow release system used in the previous experiment. MSCs were cultured for 14 days, and after the culture, cells were immunostained with osteogenic marker anti-ALP antibody (Fig. 12.10).

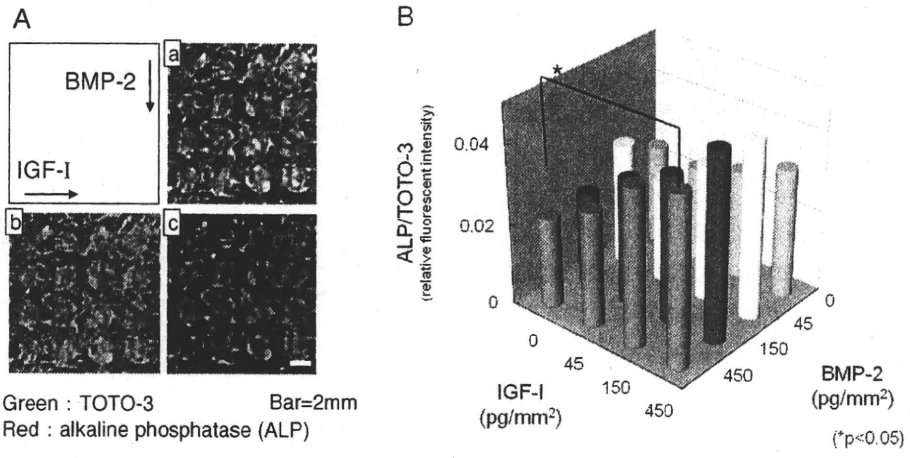

Fig. 12.10 MSC culture on growth factor array in slow-release system consisted of BMP-2 and IGF-I. (**a**) Fluorescent image of MSC cultured on growth factor array. a: Merge, b: Fluorescence image of TOTO-3 staining. C: Fluorescence image indicating osteogenic differentiation (bar: 2 mm). (**b**) ALP expression of MSC on growth factor array with slow release system (0, 45, 150, 450 pg/mm^2 of growth factors were combined) was measured by immunostaining with anti-ALP antibody. In the areas where BMP-2 was printed at concentrations of 150 and 450 pg/mm^2, osteogenic differentiation was promoted depended on IGF-I concentration

In this culture, the osteogenic differentiation was not promoted by BMP-2, but when IGF-I coexisted, osteogenic differentiation was promoted, depending on IGF-I concentration.

12.4 Discussion

12.4.1 Growth Factor Array Using Photoreactive Growth Factors

Immobilization efficiency of photoreactive growth factors was examined using [^{125}I] IGF-I. From this experiment, it was shown that the growth factors were printed with high accuracy. The immobilization efficiency decreased as the quantity of protein on the substratum increased. According to previously published work, growth factors immobilized with a phenyl-azido arm may form multi-layers on the substrata [28, 34]. This result suggests that when the quantity of the printed growth factors increases, these growth factor may form multi-layers, preventing a direct reaction with the substratum, and some of the protein may be washed away by rinsing with PBS.

To study the feasibility of the growth factor array, we first fabricated the arrays consisting of IGF-I and FGF-2 and cultured C2C12 myoblasts. We also confirmed the effect of soluble IGF-I and FGF-2 for myogenic differentiation. Several laboratories have shown that soluble IGF-I, at concentrations up to 20 ng/mL, promotes myogenic differentiation in a dose-dependent manner [35]. On the other hand, it has also been reported that FGF-2 inhibits expression of the myogenic transcription factor MyoD [8, 9, 36]. In the present work, FGF-2 inhibited the myogenin expression induced by IGF-I in a dose-dependent manner. Interestingly, soluble FGF-2 did not completely inhibit the myogenin expression. Approximately 5% of the cells remained myogenin-positive. According to the previous work, cultured muscle cells synthesize substantial amounts of IGF-I, which may cause the basal myogenin expression [37].

Compared to that of soluble growth factors, the effect of immobilized growth factors were lower. There are two possibilities for this discrepancy. The first possibility is a weakened activity of photoreactive growth factors from introducing the azido-phenyl group. In this method, the azido-phenyl group is supposed to be introduced to the amino groups of the N-terminus or to lysine residues. This chemical modification may cause conformational changes that can reduce the interaction activity with receptors. Another possibility is the restricted flexibility of immobilized growth factors due to the immobilization to the substratum via short arm, which may interfere the interaction with the receptor. Elongating the length of arm may improve the activity of immobilized growth factors.

12.4.2 Growth Factor Array Using Surface Activated Substratum

Although the use of photoreactive growth factors was one good way to immobilize growth factors on the substratum, a photoreactive arm needs to be introduced to